

# Self-stresses and Crack Formation by Particle Swelling in Cohesive Granular Media

M. S. El Youssoufi\*, J.-Y. Delenne and F. Radjai  
LMGC, CNRS-Université Montpellier II,  
Place Eugène Bataillon,  
34095 Montpellier cedex, France.

October 12, 2018

## Abstract

We present a molecular dynamics study of force patterns, tensile strength and crack formation in a cohesive granular model where the particles are subjected to swelling or shrinkage gradients. Non-uniform particle size change generates self-equilibrated forces that lead to crack initiation as soon as strongest tensile contacts begin to fail. We find that the coarse-grained stresses are correctly predicted by an elastic model that incorporates particle size change as metric evolution. The tensile strength is found to be well below the theoretical strength as a result of inhomogeneous force transmission in granular media. The cracks propagate either inward from the edge upon shrinkage and outward from the center upon swelling.

83.80.Fg, 74.80.-g, 45.70.Mg

**key words:** granular media / porous media / cohesion / shrinkage / swelling / rupture

The term “cohesive granular media” covers a vast spectrum of granular materials in which rigid grains are bound together by cohesion forces of various chemico-physical origins [Maugis, 1999]. Well-known examples are fine powders and soils with more or less colloidal or water content [Mitchell, 1993]. The solid-like behavior attributed to noncohesive granular media under quasistatic shearing [Jaeger et al., 1996] becomes the dominant feature in the presence of cohesion, with an increasing effective tensile strength as a function of the contact tensile strength [Kim and Hwang, 2003]. The stress-stain behavior and fracture mechanics of cohesive granular media raise interesting open issues from a grain-scale point of view and in interaction with heat or mass transfer.

---

\*Correspondance to: M.S. El Youssoufi (elyous@lmgc.univ-montp2.fr)

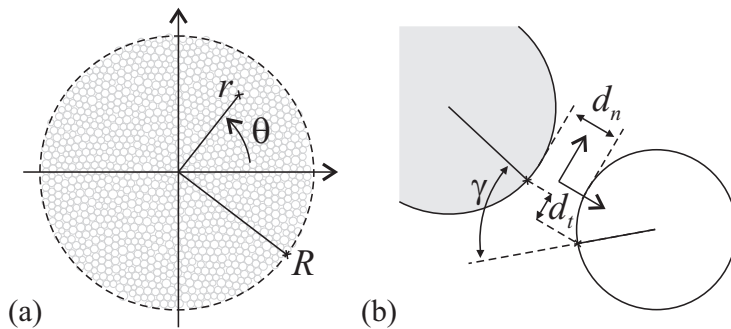


Figure 1: (a) Geometry of the sample; (b) Relative displacements between two edge points belonging to two particles and coinciding initially with their contact point.

An appealing issue is how and in which respects these “granular solids” differ from molecular solids (in the absence of a granular structure). For example, the phenomenon of stress concentration, induced by defects at different scales, governs the initiation of failure in molecular solids, the effective tensile strength remaining generally far below the “theoretical” strength [Herrmann and Roux, 1990]. In a granular assembly, stress concentration occurs already at the particle scale in the form of a highly inhomogeneous distribution of contact forces [Mueth et al., 1998, Radjai et al., 1998]. This suggests that, even in the absence of mesoscopic defects, the tensile strength will be weak compared to its theoretical value for a granular assembly (to be defined below). However, the tensile-strength properties have scarcely been analyzed from a microscopic standpoint [Kim and Hwang, 2003, Radjai et al., 2001].

In this Letter, we consider a benchmark test that was designed to probe the *intrinsic* tensile response (reflecting only the granular disorder) of a cohesive granular sample by avoiding both wall effects and strain localization as spurious sources of randomness. The sample consists of rigid cohesive disks compacted numerically into a circular form in a two-dimensional space; See Fig. 1(a). At the start, the normal force is exactly zero at all contacts. Then, the particle diameters are increased (or decreased) at a rate that depends on distance to the sample center. Such gradients of particle size change occur, for instance, in fine soils, where particle swelling (or shrinkage) happens as a result of humidification (or drying) [Mitchell, 1993]. As we shall see in detail below, this bulk straining induces a field of radial (or orthoradial) tensile self-stresses increasing in magnitude with time, and leading eventually to crack initiation at the center (or on the edge).

For the simulations, we used the molecular dynamics method with a velocity-Verlet scheme for the integration of the equations of motion [Allen and Tildesley, 1987]. Cohesive interaction between two particles implies resistance to relative motion (normal displacement  $d_n$ , tangential displacement

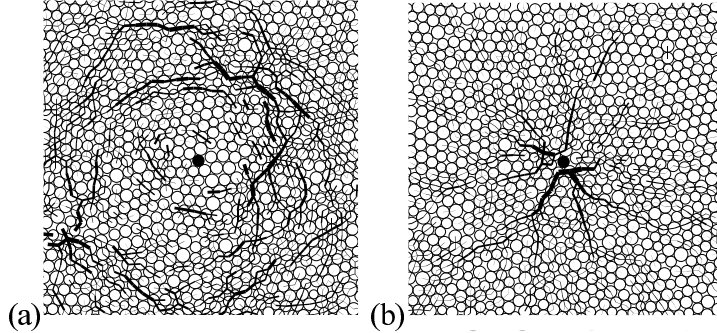


Figure 2: Tensile (a) and compressive (b) normal forces generated by the swelling of a single particle (in black). The line width is proportional to the normal force.

$d_t$  and angular displacement  $\gamma$ ) of two edge points belonging respectively to the two particles and coinciding initially with the contact point; Fig. 1(b). The corresponding contact actions are the normal force  $f_n$ , the tangential force  $f_t$  and the contact torque  $M$ . We assume a linear elastic behavior characterized by three stiffnesses  $E_n$ ,  $E_t$  and  $E_\gamma$ , so that  $f_n = E_n d_n$ ,  $f_t = E_t d_t$  and  $M = E_\gamma \gamma$ . As usual, damping actions are added in order to account for contact inelasticity and ensure numerical stability.

This elastic behavior holds as long as the contact actions remain below a “yield surface”  $\zeta = \zeta(f_n, f_t, M) = 0$ . We used the following function that fits our previous experimental tests with a particular type of glue used to stick cylindrical particles together [Delemne et al., 2002]:

$$\zeta = \left( \frac{f_n}{f_n^y} \right) + \left( \frac{f_t}{f_t^y} \right)^2 + \left( \frac{M}{M^y} \right)^2 - 1, \quad (1)$$

where  $f_n^y$ ,  $f_t^y$  and  $M^y$  are the yield parameters for normal, tangential and angular actions, respectively. The elastic domain corresponds to  $\zeta < 0$ . Note that  $f_n$  can take indefinitely large values (the positive sign corresponding to compressive forces) but it has a lower bound  $f_n = -f_n^y$  that defines the largest tensile force that can be sustained by a contact. As soon as  $\zeta \geq 0$ , the cohesive bond breaks down irreversibly and the contact turns into noncohesive frictional behavior [Luding, 1998].

In general, the shape of the yield function  $\zeta$  and the values of the parameters will influence the failure properties of the material as a whole for a specified loading path. In our system, loading by particle swelling or shrinkage induces appreciable displacements only along the contact normals. As a result, the behavior is not sensitive to the choice of the values of  $f_t^y$  and  $M^y$ , and the failure is governed by extensional strain when  $f_n^y$  is reached at a strongly tensile contact in the sample.

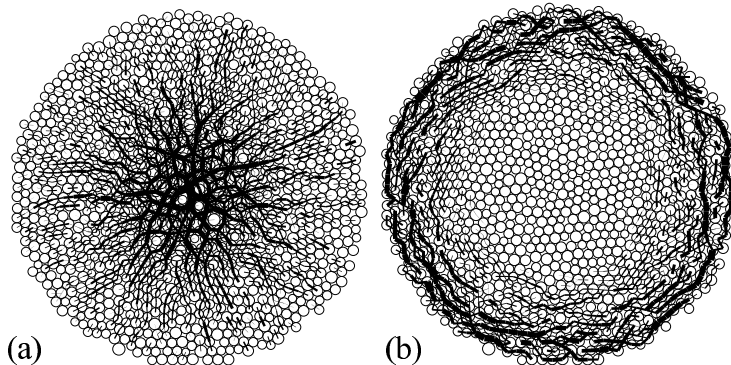


Figure 3: Compressive (a) and tensile (b) forces in a shrinkage simulation.

We used samples composed of 1133 polydisperse disks with a uniform distribution of diameters  $D$  within a range  $[D_{min}, D_{max}]$  where  $D_{max} = 1.2 D_{min}$ . The coefficient of friction is  $\mu = 0.1$ . Each sample is created by removing all particles belonging to a noncohesive assembly in static equilibrium except those contained inside a circle of radius  $R_0$ . The cohesive bonds are then switched on and the sample is allowed to relax to equilibrium. The samples prepared by this procedure correspond to a dense but disordered packing of solid fraction  $\simeq 0.89$  and coordination number 3.8.

At the beginning, the system is in its reference state with the contact actions being identically zero everywhere. Obviously, multiplying all particle diameters by the same factor does not disturb this state since no relative motions are generated at the contact points, whereas *differential* particle-size change gives immediately rise to permanent compressive and tensile force gradients. For instance, the swelling of a single particle produces compressive radial forces by pushing the neighboring particles outward, as well as tensile orthoradial forces by increasing the total length of the “rings” of contiguous particles surrounding the swelling particle; Fig. 2. A slight shrinkage of the same particle produces exactly the same force patterns with the signs inverted everywhere (compressive contacts turning to tensile, and vice versa).

Since we are interested here only in the effect of bulk straining, we require that the swelling rate  $\dot{s}_i \equiv \dot{D}_i/D_i$  of each particle  $i$  is independent of its diameter  $D_i$ . We use the simplest swelling kinetics defined by a constant gradient from the center to the edge,  $\dot{s}_i = \frac{\alpha}{R_0} r_i$ , where  $r_i$  is the distance of the particle to the system center, and  $\alpha$  is a constant rate. Positive and negative values of  $\alpha$  correspond to particle swelling and shrinkage, respectively.

Figure 3 shows snapshots of normal compressive and tensile forces in a shrinkage simulation. Although at the very local scale the forces are inhomogeneously distributed, we observe radial and orthoradial compressive forces decreasing in magnitude from the center to the edge, as well as orthoradial

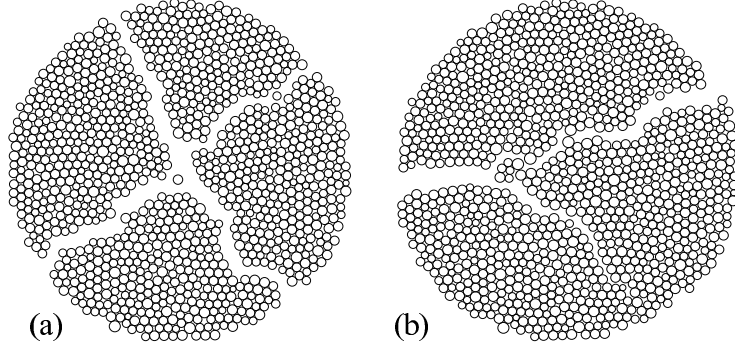


Figure 4: Crack patterns in swelling (a) and shrinkage (b) simulations.

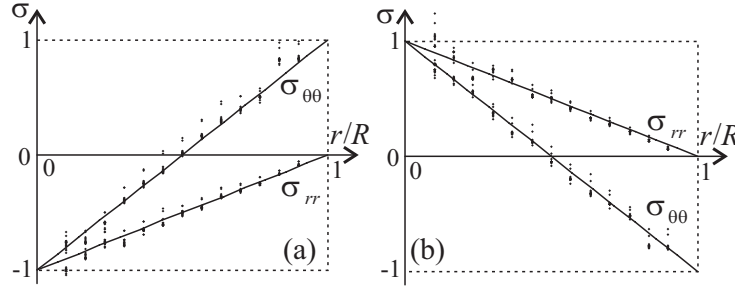


Figure 5: Normalized stress components as a function of distance  $r$  to the center in swelling (a) and shrinkage (b) simulations. The full lines are elastic fits.

tensile forces decreasing in magnitude from the edge to the center. The cracks appear on the edge as soon as the first tensile contact fails, and they propagate towards the center as shown in Fig. 4(b). In swelling simulations, the respective roles of compressive and tensile roles are simply interchanged with respect to the shrinkage case. As a result, the cracks are initiated at the center, and they propagate towards the edge; Fig. 4(a).

The coarse-grained stresses can be evaluated from the contact forces by means of the “micromechanical” expression of the stress tensor  $\boldsymbol{\sigma}$  [Christoffersen et al., 1981]:

$$\sigma_{ij} = \frac{1}{V} \sum_{c \in V} f_i^c \ell_j^c, \quad (2)$$

where  $i$  and  $j$  design the coordinates,  $V$  is the control volume over which the stress tensor is evaluated (the contacts  $c$  taken from this volume),  $f_i^c$  is the  $i$  component of the force  $\mathbf{f}^c$  at contact  $c$ , and  $\ell_j^c$  is the  $j$  component of the vector  $\boldsymbol{\ell}^c$  joining the centers of the two contact neighbors.

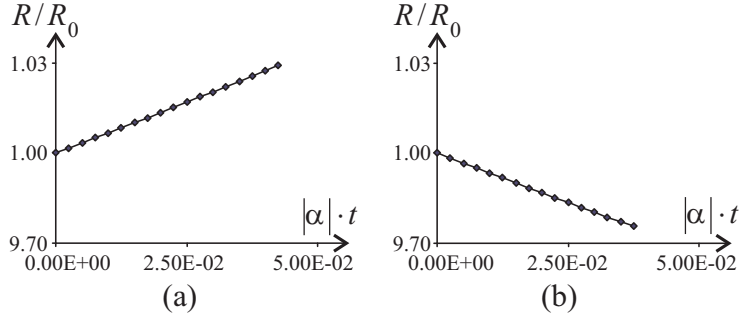


Figure 6: Evolution of the sample radius  $R$  in swelling (a) and shrinkage (b) simulations.

The stress tensor is a well-defined average if the control volume  $V$  contains a sufficiently large number of contacts. This requirement is satisfied by taking concentric circular volume elements as suggested by the rotational invariance of our system. We use polar coordinates and the radial and angular positions will be denoted by  $r$  and  $\theta$ , respectively; Fig. 1(a). As a result of isotropic straining, the cross components  $\sigma_{r\theta}$  are zero.

The radial stress  $\sigma_{rr}$  and orthoradial stress  $\sigma_{\theta\theta}$  are shown in Fig. 5(a) as a function of distance  $r$  to the center at different stages of a swelling simulation. For each data set at a given instant of evolution, we have normalized the distance  $r$  by  $R$  and the stress components by the largest tensile stress  $-\sigma_{max}$  (occurring at the center). We see that the normalized stresses collapse on a straight line as a function of  $r$  and they nicely agree with a one-parameter analytical fit that will be detailed below. Note that  $\sigma_{rr}$  is negative (tensile stress) throughout the sample, whereas  $\sigma_{\theta\theta}$  changes sign at  $r \simeq R/2$ . In the case of shrinkage simulations, similar results are obtained with opposite signs, as shown in Fig. 5(b).

We now turn to analytical evaluation of the stresses. At a coarse-grained scale, the granular assembly will be represented by a linear elastic medium with an effective stiffness  $E$  and an effective Poisson's ratio  $\nu$ . This is a plausible assumption although, as we shall see below, the behavior of the stresses as a function of  $r$  is independent of the nature of the interactions. On the other hand, coarse-grained swelling at a point  $A$  of polar coordinates  $(r, \theta)$  in space is equivalent to an imposed isotropic *space dilation*  $\dot{s}(r, \theta) = \langle \dot{s}_i \rangle_{i \in V(r, \theta)}$ , where the average is taken over all particles contained in a representative volume  $V(r, \theta)$  centered on  $A$ . Since the rates are independent of particle diameters, we get

$$\dot{s} = \frac{\alpha}{R_0} r. \quad (3)$$

Then, the strain-rate tensor  $\dot{\epsilon}$  at a point is the sum of two terms:

$$\dot{\epsilon} = \dot{\epsilon}^e + \dot{s}\mathbf{I}, \quad (4)$$

where  $\dot{\epsilon}^e$  is the elastic strain rate,  $\mathbf{I}$  represents the unit tensor, and  $\dot{s}\mathbf{I}$  is the metric change rate.

We assume that the displacement field  $\mathbf{u}(r, \theta)$  is radial (according to the symmetry of straining expressed by Eq. 3 and that of the sample) so that  $\dot{\epsilon}_{r\theta} \equiv 0$ . Since the radius  $R$  of the sample changes with time, Hooke's laws will be written in the form of rate equations:

$$\begin{cases} \dot{\epsilon}_{rr}^e &= \dot{\epsilon}_{rr} - \dot{s} &= -\frac{1}{E}(\dot{\sigma}_{rr} - \nu \dot{\sigma}_{\theta\theta}), \\ \dot{\epsilon}_{\theta\theta}^e &= \dot{\epsilon}_{\theta\theta} - \dot{s} &= -\frac{1}{E}(\dot{\sigma}_{\theta\theta} - \nu \dot{\sigma}_{rr}), \end{cases} \quad (5)$$

where extensional strains and compressive stresses are counted positive. We need also the balance equation which takes the following form in polar coordinates:

$$\dot{\sigma}_{\theta\theta} - \dot{\sigma}_{rr} = r \frac{\partial \dot{\sigma}_{rr}}{\partial r}. \quad (6)$$

The set of equations 3, 5 and 6 is easily integrated over time and space using the boundary conditions  $\mathbf{u}(r = 0) = 0$  (imposed by 3) and  $\sigma_{rr}(r = R) = 0$  (by continuity of the normal stress at the boundary). The solution is

$$\begin{cases} R &= \frac{R_0}{1-2\alpha t/3}, \\ \sigma_{rr} &= E \left(1 - \frac{R_0}{R}\right) \left(\frac{r}{R} - 1\right), \\ \sigma_{\theta\theta} &= E \left(1 - \frac{R_0}{R}\right) \left(2\frac{r}{R} - 1\right). \end{cases} \quad (7)$$

We see that both stress components are linear in  $r$ . The simulation data of Fig. 5 were fitted by adjusting only the effective elastic modulus  $E$ . The evolution of the system is, however, nonlinear as a function of time. The evolution of  $R$  is shown in Fig. 6 for swelling ( $\alpha > 0$ ) and shrinkage ( $\alpha < 0$ ) simulations together with the analytical fit from Eq. 7 which involves no fitting parameter. The agreement is excellent although the nonlinear nature of the evolution can not be seen for  $|\alpha|t \ll 1$ . The largest tensile stress  $\sigma_{max}$  occurs on the edge for shrinkage and at the center for swelling. From Eq. 7, we get  $\sigma_{max} = \frac{2}{3}E |\alpha|t$ . Again, this linear form nicely fits the evolution of  $\sigma_{max}$  (by virtue of the fits shown in Fig. 5) up to failure for  $\sigma_{max} = \sigma^y$ . The latter represents the effective tensile strength of the material.

It is worth noting that, Poisson's ratio  $\nu$  does not appear in Eqs. 7 and the only role of the stiffness  $E$  is to set the stress scale. This means that the behavior of the stress components and and sample size as a function of  $r$  is independent of the local force law. In particular, in the limit of infinitely rigid particles, the same results remain true up to a stress scale which may be fixed through a confining pressure. More generally, both the local interactions and the mass or heat transfer influence the stress scale.

By analogy with molecular solids, we introduce a "theoretical" tensile strength  $\sigma_{th}^y$  based on the interactions between two particles [Herrmann and Roux, 1990]. According to Eq. 2, the orthoradial stress is  $\sigma_{\theta\theta} = n_c \langle f_{\theta\ell\theta} \rangle \simeq n_c \langle \ell \rangle \langle f_{\theta} \rangle$ , where  $n_c$  is the density of contacts and  $\langle \dots \rangle$  designs averaging over the control volume. The largest value of  $\sigma_{\theta\theta}$  in tension corresponds to the limit where all forces are polarized in the same direction and

they have all reached the largest tensile force  $f_n^y$ . This defines the “theoretical” tensile strength

$$\sigma_{th}^y = n_c \langle \ell \rangle f_n^y \quad (8)$$

In our simulations, the measured tensile strength  $\sigma^y$  is by a factor  $\simeq 4.3$  below  $\sigma_{th}^y$ . In molecular solids, a similar discrepancy between  $\sigma_{th}^y$ , defined from atomic interactions in a regular atomic arrangement, and  $\sigma^y$  stems from “built-in” disorder at different scales leading to stress concentration. In a granular solid, the disorder is “intrinsic” to the structure. As a result, the contact forces both in cohesive and noncohesive granular media have a wide distribution with a decreasing exponential shape for strong forces [Radjai et al., 1998, Radjai et al., 2001]. It seems that  $\sigma^y$  reflects the *strongest* contact force at failure, whereas  $\sigma_{th}^y$  represents the *mean* tensile force by construction. Indeed, the strongest tensile force in simulations is by a factor  $\simeq 5$  below the mean tensile force, and this is close to  $\sigma_{th}^y/\sigma^y \simeq 4.3$ . As far as we know, this is the first example showing how the local force inhomogeneities in a granular material control a macroscopic property, namely the tensile strength.

In summary, our numerical data and their comparison with an analytical evaluation of stresses in the elastic domain and at failure suggest that a macroscopically elastic behavior is relevant up to crack initiation, as in molecular solids. However, the tensile strength is dependent on the inhomogeneous transmission of forces. The simple test described in this Letter not only provides reproducible results, but it has also the advantage of combining features of discrete modeling with theoretical predictability at the macroscopic scale.

This approach may now be used to investigate and to predict the tensile thresholds and crack propagation in cohesive granular materials as a function of the initial density and anisotropy of the material or the possible couplings of the local cohesion with mass and heat transfer in the pores as in fine soils and granular rocks [Tarbuck and Lutgens, 2002]. The theoretical approach can be extended to other structured media involving mesoscopic length scales, such as gels [Mrani et al., 1995], cellular media [Schwarz and Safran, 2002], layered structures such as wood [Kübler, 1987] and pastes [Ponsart et al., 2003]. Swelling or shrinkage may occur as a result of cellular growth (in biological systems) or the evolution of local variables such as water content and temperature.

It is a pleasure to thank J.-C. Bénéat and J. N. Roux for helpful suggestions.

## References

- [Allen and Tildesley, 1987] Allen, M. P. and Tildesley, D. J. (1987). *Computer Simulation of Liquids*. Oxford University Press, Oxford.
- [Christoffersen et al., 1981] Christoffersen, J., Mehrabadi, M. M., and Nemat-Nasser, S. (1981). *J. Appl. Mech.*, 48:339–344.



- [DeLenne et al., 2002] DeLenne, J.-Y., Youssoufi, M. S. E., and Bénét, J.-C. (2002). Comportement mécanique et rupture de milieux granulaires cohésifs. *C.R. Mécanique*, 330:475–482.
- [Herrmann and Roux, 1990] Herrmann, H. J. and Roux, S., editors (1990). *Statistical models for fracture in disordered media*, Amsterdam. North Holland.
- [Jaeger et al., 1996] Jaeger, H. M., Nagel, S. R., and Behringer, R. P. (1996). Granular solids, liquids, and gases. *Reviews of Modern Physics*, 68(4):1259–1273.
- [Kim and Hwang, 2003] Kim, T.-H. and Hwang, C. (2003). Modelling of tensile strength on moist granular earth material at low water content. *Engineering Geology*, 69:233–244.
- [Kübler, 1987] Kübler, H. (1987). Growth stresses in tree stems and related wood properties. *Forest Products Abstracts*, 10:61–119.
- [Luding, 1998] Luding, S. (1998). Collisions & contacts between two particles. In Herrmann, H. J., Hovi, J.-P., and Luding, S., editors, *Physics of dry granular media - NATO ASI Series E350*, pages 285–304, Dordrecht. Kluwer Academic Publishers.
- [Maugis, 1999] Maugis, D. (1999). *Contact, Adhesion and Rupture of Elastic Solids*. Springer, Berlin, Germany.
- [Mitchell, 1993] Mitchell, J. K. (1993). *Fundamentals of Soil Behavior*. Wiley, New York, USA.
- [Mrani et al., 1995] Mrani, I., Bénét, J.-C., and Fras, G. (1995). Transport of water in a biconstituent elastic medium. *Appl. Mech. Rev.*, 48:717–721.
- [Mueth et al., 1998] Mueth, D. M., Jaeger, H. M., and Nagel, S. R. (1998). Force distribution in a granular medium. *Phys. Rev. E.*, 57(3):3164–3169.
- [Ponsart et al., 2003] Ponsart, G., Vasseur, J., Frias, J. M., Duquenoy, A., and Méot, J. (2003). Modelling of stress due to shrinkage during drying of spaghetti. *Journal of Food Engineering*, 57:277–285.
- [Radjai et al., 2001] Radjai, F., Preechawuttipong, I., and Peyroux, R. (2001). Cohesive granular texture. In Vermeer, P., Diebels, S., Ehlers, W., Herrmann, H., Luding, S., and Ramm, E., editors, *Continuous and discontinuous modelling of cohesive frictional materials*, pages 148–159, Berlin. Springer Verlag.
- [Radjai et al., 1998] Radjai, F., Wolf, D. E., Jean, M., and Moreau, J.-J. (1998). Bimodal character of stress transmission in granular packings. *Phys. Rev. Lett.*, 80(1):61–64.
- [Schwarz and Safran, 2002] Schwarz, U. S. and Safran, S. A. (2002). Elastic interactions of cells. *Phys. Rev. Lett.*, 88:048102.

[Tarbuck and Lutgens, 2002] Tarbuck, E. J. and Lutgens, F. K. (2002). *Earth: An Introduction to Physical Geology*. Pearson Education, Inc., New Jersey.